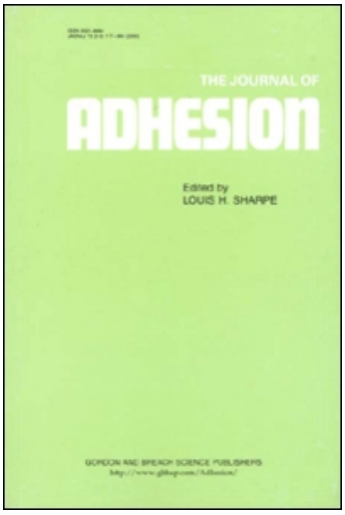

The Journal of Adhesion
Publication details, including instructions for authors and subscription information:
http://www.informaworld.com/smpp/title~content=t713453635

Effect of Surface Roughness on the Performance of Adhesive Joints Under Static and Cyclic Loading

S. Azari[a]; M. Papini[b]; J. K. Spelt[a]
[a] Department of Mechanical and Industrial Engineering, University of Toronto, Toronto, Ontario, Canada [b] Department of Mechanical and Industrial Engineering, Ryerson University, Toronto, Ontario, Canada

Online publication date: 10 August 2010

To cite this Article Azari, S. , Papini, M. and Spelt, J. K.(2010) 'Effect of Surface Roughness on the Performance of Adhesive Joints Under Static and Cyclic Loading', The Journal of Adhesion, 86: 7, 742 — 764
To link to this Article: DOI: 10.1080/00218464.2010.482430
URL: http://dx.doi.org/10.1080/00218464.2010.482430

The Journal of Adhesion, 86:742–764, 2010

ISSN: 0021-8464 print/1545-5823 online
DOI: 10.1080/00218464.2010.482430

Taylor & Francis
Taylor & Francis Group

Effect of Surface Roughness on the Performance of Adhesive Joints Under Static and Cyclic Loading

S. Azari[1], M. Papini[2], and J. K. Spelt[1]
[1]Department of Mechanical and Industrial Engineering, University of Toronto, Toronto, Ontario, Canada
[2]Department of Mechanical and Industrial Engineering, Ryerson University, Toronto, Ontario, Canada

The role of surface roughness on the fatigue and fracture behavior of a toughened epoxy adhesive system was investigated experimentally. Fatigue studies covered both the fatigue threshold strain energy release rate, G_{th}*, and fatigue crack growth rates, while the strain energy release rate for crack initiation,* G_c^i*, and the steady-state value,* G_c^s*, were measured under quasi-static loading. Mixed-mode fatigue results showed a significant dependency on surface roughness.* G_{th} *increased with roughness, reached a plateau, and then decreased for very rough surfaces. This increase in* G_{th} *was explained in terms of the increase in bonding and fracture surface area, crack growth retardation due to the microtopography of the substrate, and crack path deviation from the interface. The decrease in* G_{th} *for very rough substrates was attributed to void formation and stress concentration at the tip of asperities. The effect of roughness on fatigue diminished as the applied strain energy release rate increased. This was a result of the crack path becoming more cohesive, moving away from the interface. Similarly, no effect of surface roughness was observed in the mode-I fatigue results and the mixed-mode fracture results, since the crack path in these cases was far enough from the interface.*

Keywords: Epoxy adhesive; Fatigue crack growth; Fatigue threshold; Quasi-static fracture; Surface roughness

Received 23 October 2009; in final form 4 February 2010.
One of a Collection of papers honoring David A. Dillard, the recipient in February 2010 of *The Adhesion Society Award for Excellence in Adhesion Science, Sponsored by 3M*.

Address correspondence to J. K. Spelt, Department of Mechanical and Industrial Engineering, University of Toronto, 5 King's College Road, Toronto, Ontario, Canada M5S 3G8. E-mail: spelt@mie.utoronto.ca

ABBREVIATIONS

a	Crack length
A_r	Projected (apparent) profile area
B	Specimen width
C	Joint compliance
$c_1 - c_4$	Regression coefficients for normalized crack length *versus* compliance equation
d	Crack tip distance from the thinner arm of an ADCB
E	Tensile elastic modulus of adherends
E_a	Tensile elastic modulus of adhesive
G	Strain energy release rate
G_I	Mode I strain energy release rate
G_{II}	Mode II strain energy release rate
G_c	Critical strain energy release rate under quasi-static loading
G_c^i	Crack initiation strain energy release rate under quasi-static loading
G_c^s	Steady-state critical strain energy release rate under quasi-static loading
G_{th}	Fatigue threshold strain energy release rate
h	Adherend thickness
h_l	Lower adherend thickness
h_u	Upper adherend thickness
L_{rl}	Ratio of the actual to the projected profile length in longitudinal direction
L_{rw}	Ratio of the actual to the projected profile length in transverse direction
N	Number of cycles
P	Force per unit width
R	Displacement ratio in a fatigue cycle
R_a	Arithmetic average of the roughness profile
R_{lo}	Developed length of the roughness profile, based on ISO 4287
t	Adhesive thickness
w	Specimen length

Greek symbols

δ_{min}	Minimum displacement in a fatigue cycle
δ_{max}	Maximum displacement in a fatigue cycle
σ_y	Yield stress
ψ	Phase angle

1. INTRODUCTION

Bonding surfaces are often abraded to remove weak or contaminated areas and to increase mechanical interlocking and the effective bonding area. For example, grit blasting can produce a significant improvement in joint strength on aluminum surfaces, although bond strength did not continue to increase with further roughening [1,2]. In contrast, Shahid and Hashim [3] found a linear relation between surface roughness and the cleavage strength of steel adhesive joints. Zhang *et al.* [4] measured a continuous increase in the interfacial fracture resistance of aluminum layered double cantilever beam joints bonded using an epoxy adhesive. Carbon/epoxy composite single lap shear joints also showed a continuous increase in the bond strength with adherend roughness [5]. The tensile strength of aluminum lap shear joints bonded using an epoxy resin showed an increase with roughness, but reached a constant value at an average roughness, S_a, of 3 μm [6]. Steel tubular single lap joints showed the highest static shear strength at R_a between 1.5 and 2.0 μm, becoming weaker as the bonding surfaces were made rougher still [7]. Uehara and Sakurai [8] found different levels of optimum roughness for the tensile strength of epoxy and cyanoacrylate adhesive joints bonding steel. They also conducted shear and peel tests, finding that the effect of roughness was smaller in shear and disappeared altogether in the peel tests [8].

Surface roughness was also found to influence the fatigue life of steel tubular single lap joints subjected to a cyclic torque [9]. The fatigue strength increased up to an average roughness, R_a, of 1.5–2 μm, and then decreased suddenly as the roughness was increased to 3 μm. The failure surface at $R_a = 0.6$ μm was fully interfacial, but was partially cohesive at $R_a = 2.0$ μm. Similar torsional fatigue tests have yielded a range of optimum roughness values depending on the adhesive system [7,10]. The stress analysis of Kwon and lee [10] suggested that the optimum roughness depends on the adhesive layer thickness. The fatigue threshold, G_{th}, of aluminum cracked lap-shear joints was increased by more than 80% as the adherend roughness was increased from $R_a = 0.77$ μm to 1.33 μm [11]. This was attributed to the increase in the surface area and the change in the failure mode from interfacial at $R_a = 0.77$ μm to cohesive at $R_a = 1.33$ μm.

A wide variety of explanations have been proposed for the positive and negative effects of increasing surface roughness: an increase in the bonding area [3–6,8,12], increased mechanical interlocking [5], a reduction in wettability by the adhesive [6], the deviation of crack path away from a weaker interfacial region [3,5,12,13], and an increase in

stress concentration at asperity tips [14]. While there has been considerable work on the effect of surface roughness on the fracture behavior of adhesive joints, relatively few papers have studied the effect of roughness on fatigue behavior and no published work exists on the relationship between the fatigue threshold and surface roughness. This case is of particular interest, because recent work has shown that fatigue crack paths move even closer to the interface as the crack speed decreases [11,15]. This paper presents experimental data concerning the effect of surface roughness on the fatigue threshold and fatigue crack growth rates of aluminum-epoxy joints under both Mode I and mixed-mode loading. The results are compared with quasi-static mixed-mode fracture measurements of both the crack initiation and steady-state strain energy release rates.

2. EXPERIMENTAL APPROACH

2.1. Specimen Preparation

A highly-toughened, single-part epoxy adhesive was used to bond aluminum double cantilever beam (DCB) and asymmetric double cantilever beam (ADCB) specimens, which were used for Mode I and mixed-mode loading, respectively. The geometries of the joints are shown in Fig. 1. Specimens were fabricated from 12.7×19.05 mm (1/2 in $\times$ 3/4 in); and 25.4×19.05 mm (1/2 in $\times$ 3/4 in); AA6061-T651 flat bars. An adhesive

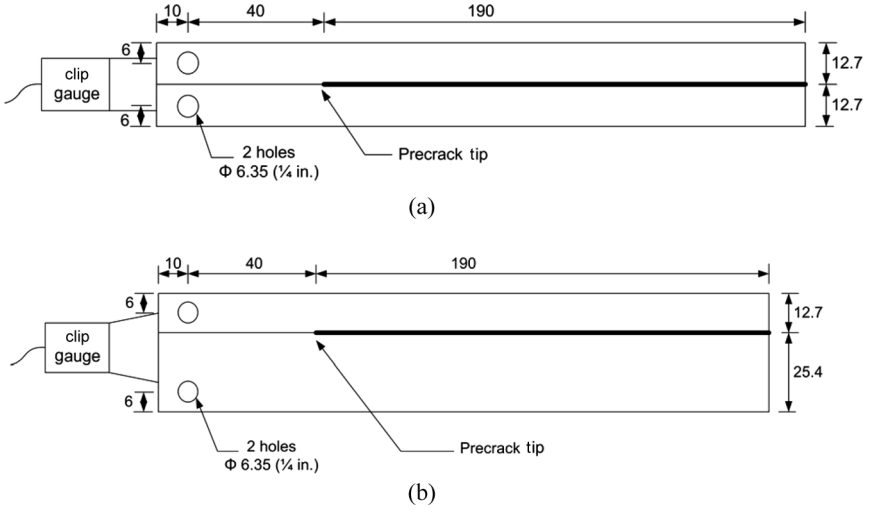

FIGURE 1 Geometry of (a) DCB (Mode I) and (b) ADCB (mixed mode) joints.

bondline thickness of 380 μm was established using spacing wires in the bondline. Prior to bonding, the adherends were roughened as described below, and then washed with running tap water and a cotton cheesecloth, and dried for 30 min at 55°C. The aluminum bars were then pretreated using the P2 etching process [16], *i.e.*, degreased with acetone and etched using an aqueous solution of ferric sulfate and sulphuric acid. Prior to applying the adhesive, the aluminum bars were rinsed using distilled water and dried at 55°C for 30 min. In order to promote wetting, the adhesive viscosity was reduced prior to application by preheating it to 55°C for 1 h. A thermocouple embedded in the bondline was used to ensure that the adhesive was cured for at least 30 min at 180°C. Excess adhesive was removed from the sides of the joint after curing using a disc sander with water as a coolant, followed by gentle sanding using a belt sander and 120-grit paper. To improve the visibility of the crack and remove any surface damage, the sides of the joint were finally sanded with 600-grit sandpaper, and a thin coating of diluted white correction fluid was applied. Five different roughnesses were produced as follows:

- Abrading with an orbital sander using a silicon carbide nylon mesh abrasive pad produced an average roughness $R_a = 1.3\,\mu m$.
- An orbital sander with a P60-grit sandpaper produced an average roughness $R_a = 1.9\,\mu m$.
- Using grinder discs with grits P80, P36, and P16 resulted in average roughnesses of 3.9, 6.4, and 9.0 μm, respectively, measured along the length of the specimen. The grinding discs were held so that the scratches produced in the surface were perpendicular to the length of the specimen.

A summary of the roughnesses and the approaches used is given in Table 1. The area scans and the surface roughness measurements

TABLE 1 Surface Roughness of Aluminum Bars Produced using Different Roughening Approaches. Four Measurements were Performed for Each Roughness. "SD" is Standard Deviation. Roughness Measurements were in the Longitudinal Direction Along the Bars with a Scan Length of 15 mm

$R_a \pm$ SD (μm)	Apparatus	Paper
1.3 ± 0.2	Orbital finisher	Silicon carbide nylon mesh abrasive pad
1.9 ± 0.1	Orbital sander	P60 sandpaper
3.9 ± 0.2	Grinder	P80 grinding disc
6.4 ± 0.6	Grinder	P36 grinding disc
9.0 ± 0.3	Grinder	P16 grinding disc

were performed using an optical profilometer (Nanovea ST 400, Microphotonics Inc., Irvine, CA, USA). Roughness was measured in a longitudinal direction along the bars, *i.e.*, in the crack growth direction. The repeatability of the roughening process was found to be satisfactory among the four samples produced at each roughness. The average roughness calculated from four measurements on any one specimen showed no statistically significant difference (t-test, 95% confidence) with the grand average, R_a, of the four specimens. The data of Table 1 are for measurements performed on a single specimen and measured prior to the etching. It was found that P2 etch did not significantly change the R_a of the aluminum surfaces (t-test, 95% confidence). Figure 2 shows the two-dimensional and three-dimensional topographies of the roughened surfaces over a scan area of 10×10 mm. Remnants of the original microtopography of the extruded aluminum surface can be seen at $R_a = 1.3\,\mu$m. The orbital sanding using the P60-grit sandpaper ($R_a = 1.9\,\mu$m) produced a uniform microtopography. The grooves formed by the grinding disc are evident in Figs. 2(c)–(e).

2.2. Fatigue Testing

All fatigue experiments were carried out at a cyclic frequency of 20 Hz, under displacement control, with a constant displacement ratio, $R = \delta_{min}/\delta_{max} = 0.1$. Previous work has shown that fatigue testing under force and displacement control yields very similar results [11], but displacement control threshold testing is easier to control and usually requires less time. A dry condition (11–15% relative humidity) was achieved by performing the experiments in a desiccant chamber. The fatigue tests began with an applied load producing the highest G of interest, and the crack slowed to the threshold value (10^{-6} mm/cycle) as the displacement was held constant.

The unloading joint compliance approach [17] was used to measure the fatigue crack length. The joint compliance was measured during the unloading portion of the cycle using the load cell output and a clip gauge attached to the end of the specimen. A CCD camera (2-mm field of view) on a motorized linear stage was used to measure the crack length and relate it to the measured joint compliance for a given specimen type using the approach of Ref. [18]. A least squares regression was used to fit a third-order polynomial to the normalized crack length, a/w, *versus* the normalized specimen compliance, CEB, for fatigue joints:

$$a/w = c_1 \times (CEB)^3 + c_2 \times (CEB)^2 + c_3 \times (CEB) + c_4, \qquad (1)$$

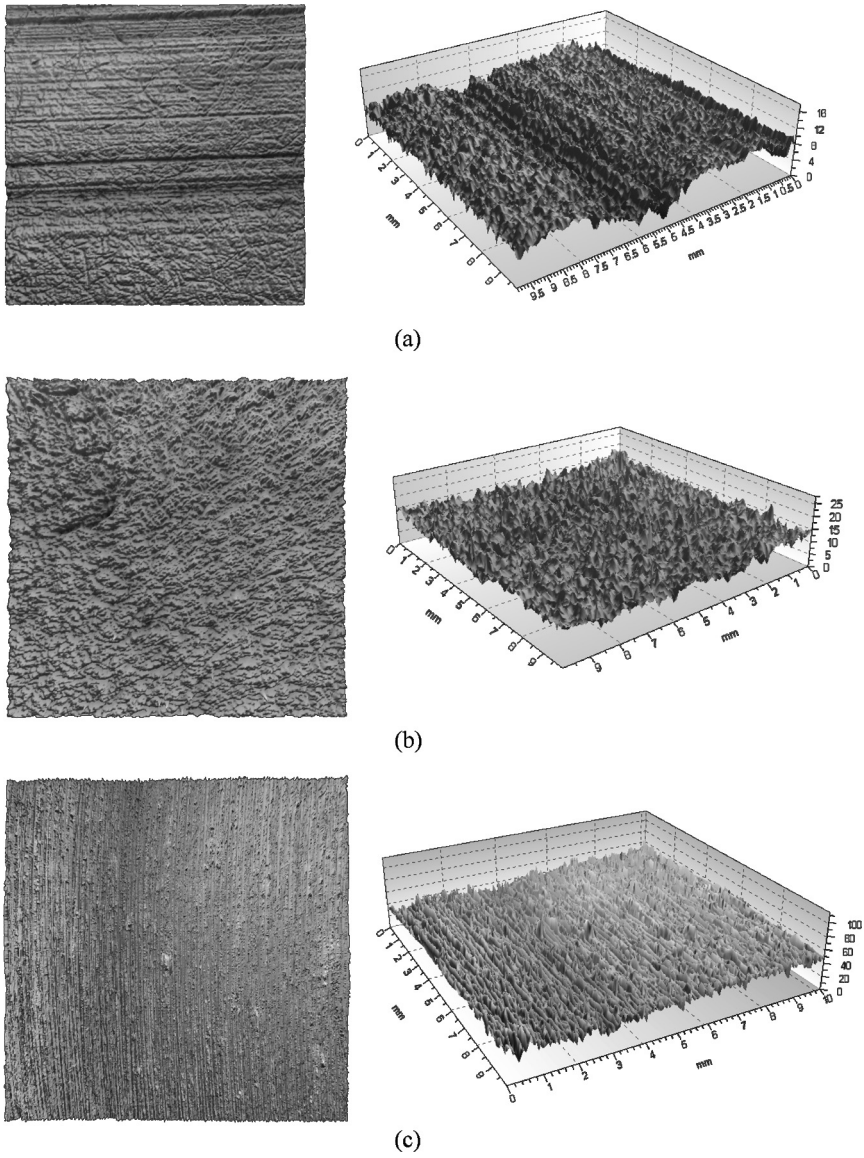

FIGURE 2 The micrographs and 3-D images of the aluminum bars with surface roughnesses of: (a) 1.3 μm, (b) 1.9 μm, (c) 3.9 μm, (d) 6.4 μm, and (e) 9.0 μm. The vertical axis in the 3-D topographies is in μm. Scan area was 10×10 mm. The direction of crack growth and roughness measurement in the micrographs was from right to left.

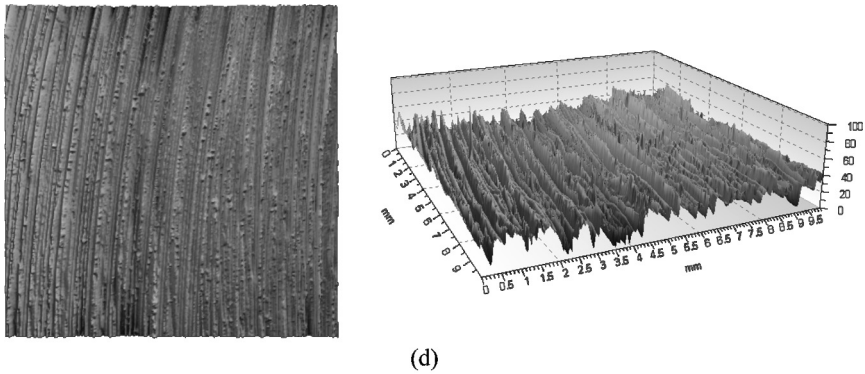

(d)

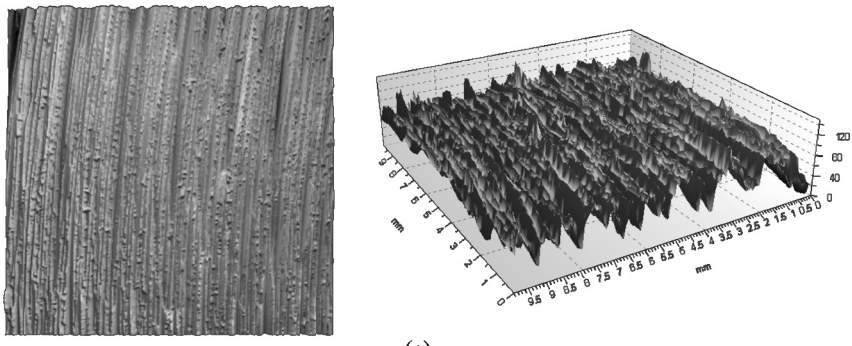

(e)

FIGURE 2 Continued.

where a is the crack length, w is the specimen length from the loading pins, C is the compliance, E is the tensile modulus of the adherends, and B is the specimen width. c_1 to c_4 are the regression fit constants.

2.3. Fracture Testing

The fracture tests were performed on the aluminum ADCB joints. The same load was applied on both arms of the ADCB to produce a mixed-mode loading condition ($\psi = 18^\circ$) at the crack tip [19]. The phase angle is a measure of the mode ratio of loading defined as $|\psi| = \arctan(\sqrt{G_{II}/G_I})$, where G_I and G_{II} are the Mode I and II components of the strain energy release rate. The ADCB specimens were loaded with a constant cross-head speed of 1 mm/min. The crack length was measured from the center of the loading pins using a microscope mounted on a micrometer stage with a resolution of 0.01 mm. Crack growth was stable in this system so that many crack

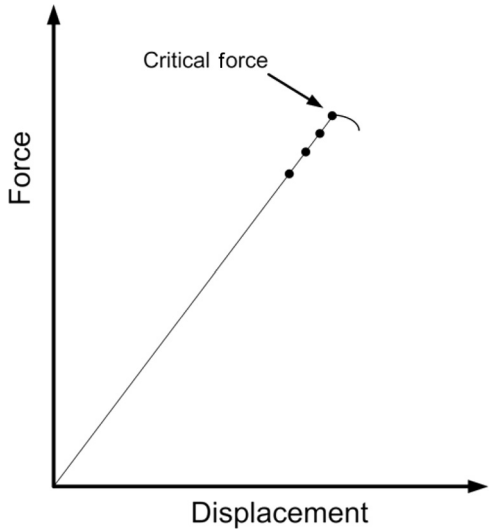

FIGURE 3 Schematic illustration of the force *vs*. displacement during loading in order to determine the quasi-static critical force for fracture tests. Black dots indicate the instances when the actuator was stopped momentarily to determine whether the load dropped at a constant displacement.

extension events could be recorded with a single ADCB specimen. To measure the critical load at each crack length, the cross-head displacement was started and stopped repeatedly in the vicinity of the expected fracture load (each time at a constant crosshead speed of 1 mm/min) until a drop in the applied load was observed (Fig. 3). Each start-stop cycle lasted for about 3 sec, with the load increment between each cycle being in the range of 20–30 N. This maximum load prior to the drop was taken as the critical fracture load for the measured crack length if visual inspection through the microscope confirmed that the macro-crack had propagated. After measuring the new macro-crack length, the ADCB was unloaded and the same procedure was followed again beginning at the new crack length.

2.4. Strain Energy Release Rate Calculation

The strain energy release rate, G, for DCB and ADCB joints was calculated from the measured force and crack length using an analytical beam-on-elastic-foundation model [15] as follows:

$$G = 12(P\alpha)^2(A + B), \tag{2}$$

where

$$A = \frac{1}{2E_u h_u^3}\frac{1}{(1-t_l/h_u)^3}\left[1+0.667\{(1-t_l/h_u)^3[1+t_l/h_u(2E_u/E_a-1)]\}^{0.25}\frac{h_u}{a}\right]^2,$$
$$B = \frac{1}{2E_l h_l^3}\frac{1}{(1-t_u/h_l)^3}\left[1+0.667\{(1-t_u/h_l)^3[1+t_u/h_l(2E_l/E_a-1)]\}^{0.25}\frac{h_l}{a}\right]^2, \quad (3)$$

and P is the force per unit width, E is the elastic modulus, t is the adhesive thickness, and h is the adherend thickness. The subscripts a, u, and l refer to the adhesive and the upper and lower substrates, respectively.

The model predicted that G values for aluminum and steel DCB and ADCB joints were within 2% of those predicted using a two-dimensional elasto-plastic finite element model (Section 3.1.2) for crack lengths of 40–120 mm [15].

3. EFFECT OF SURFACE ROUGHNESS ON FATIGUE BEHAVIOR

3.1. Mixed-Mode ADCB Specimens

Aluminum ADCB joints were chosen to study the effect of surface roughness under a mixed-mode loading condition ($\psi = 18°$). Since the Mode II component in an ADCB joint will tend to move the crack path toward the more strained adherend [15] (*i.e.*, the thinner one), it was expected that the fatigue behavior under mixed-mode conditions would be influenced by the surface roughness on the thinner adherend.

The surface roughness had a pronounced effect on the fatigue threshold under the mixed-mode condition, as seen in Fig. 4, where the solid symbols show G_{th} as calculated in the conventional way using the apparent crack surface area (the product of the specimen width and the crack growth length). The meaning of the open symbols is discussed in the next section. The rising trend, the plateau, and the decreasing trend of Fig. 4 were statistically significant (t-test, 95% confidence)—*i.e.*, proceeding left to right on Fig. 4, the G_{th} values at $R_a = 1.3\,\mu m$ and $R_a = 1.9\,\mu m$ were statistically indistinguishable [121 ± 12 and $144 \pm 30\,J/m^2$ ($\pm$standard deviation)]; both of these

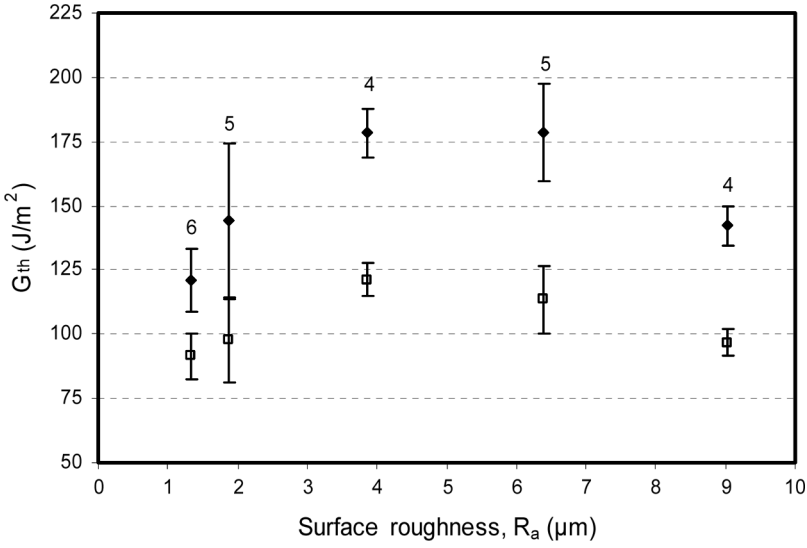

FIGURE 4 Effect of surface roughness on G_{th} of aluminum ADCB joints. Error bars show ± 1 standard deviation. The number of experiments is given above each data point. The solid symbols show G_{th} calculated conventionally using the nominal, apparent crack surface area and the open symbols show G_{th} calculated using the actual fracture surface area measured using the optical profilometer.

G_{th} values were smaller than the values at $R_a = 3.9$ and $6.4\,\mu m$ (178 ± 10 and $178 \pm 19\,J/m^2$) and these maximum values of G_{th} were, in turn, larger than the value for the roughest surface, $R_a = 9.0\,\mu m$ ($142 \pm 8\,J/m^2$).

In all of these experiments the crack path was within the adhesive, but close to the interface of the thinner adherend. This had been verified in earlier fatigue threshold testing with this same adhesive system at $R_a = 1.3\,\mu m$ using XPS (x-ray photoelectron spectroscopy) surface analysis [15].

3.1.1. Bonding Area and Fracture Surface Area

Increasing surface roughness increases the mechanical interlocking between the adhesive and the adherend and the area available for bonding. These effects were investigated using the optical profilometer to make line scans on the roughened surfaces in the longitudinal and transverse directions with measurement points every $0.5\,\mu m$. As with the roughness measurements, these scans were made on the aluminum bars prior to etching. L_{rl} and L_{rw} were defined as the ratio of

the actual profile length to the projected profile length in the longitudinal and transverse directions, respectively. This is similar to the definition of R_{lo} based on ISO 4287-1:1984 [20]. The ratio of the actual surface area to the projected (apparent) profile area, A_r, was estimated by multiplying L_{rl} and L_{rw}. R_{lo}^2, measured in the longitudinal direction, has been used as a measure of the change in the bonding area with surface roughness [3].

Figure 5 shows that L_{rl}, L_{rw}, and A_r increased with increasing R_a, and did not display the maximum seen in the G_{th} *vs* R_a trend of Fig. 4. Therefore, although the increase in bonding area may contribute to the initial increase of G_{th} with R_a, it cannot explain the existence of a maximum.

When the crack is very close to the interface, such as in the present mixed-mode case, an increase in the surface roughness can force the crack path to become more three-dimensional as it encounters asperities, thereby increasing the actual fracture surface area and possibly pinning the crack, retarding its advance. Both effects would increase the apparent strain energy release rate required to grow the crack. However, these effects should also be proportional to L_{rl}, L_{rw}, and A_r, and, therefore, increase monotonically with increasing R_a. Hence, although it may contribute to the observed increase in G_{th} with the smaller R_a (Fig. 4), it also does not explain the observed maximum.

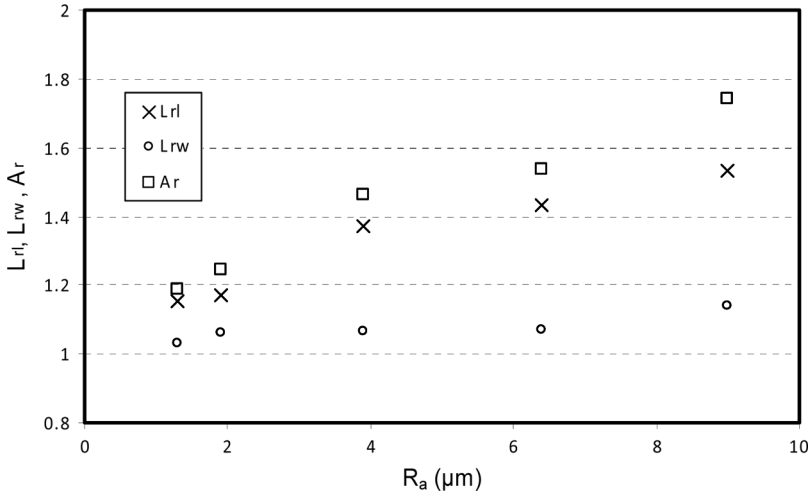

FIGURE 5 L_{rl}, L_{rw}, and A_r as a function of R_a. Points are the average of four measurements for a scan length of 15 mm. The standard deviation was approximately 4% of the average for measurements at each R_a.

It was of interest to determine how much of the increase in G_{th} was due to an increase in the actual fracture surface area compared with the apparent area (*i.e.*, width of the specimen times the crack extension). The actual fracture surface area was measured using the optical profilometer to obtain L_{rl} and L_{rw} on the residual adhesive on the fracture surface in the threshold region of a specimen. For each tested specimen, three line scans were performed at the threshold along the width and length of the specimen. A_r was calculated from the average L_{rl} and L_{rw}. For each R_a, G_{th} was then recalculated using A_r instead of the apparent crack area as shown in Fig. 4. As expected, G_{th} decreased because the actual fracture area increased, and the effect of R_a became smaller, but did not disappear. For instance, the previously observed 55% increase in G_{th} by increasing R_a from 1.3 to 3.9 μm was reduced to 32% when the actual fracture area was used. Therefore, the effect of increasing roughness may be partially due to the change in the fracture surface area, but other factors such as crack pinning must also play a role.

3.1.2. Crack Path

Figure 6 compares the fracture surfaces on the thinner arm of the aluminum ADCB joints for $R_a = 1.3$ and 6.4 μm. It is seen that increasing the roughness increased the amount of residual adhesive, *i.e.*, resulted in a more cohesive failure. This observation is consistent with other literature results where an improvement in the fracture behavior due to an increase in surface roughness was attributed to the deflection of the crack path away from the interface and a consequent increase in the residual adhesive thickness [13,14]. It has been proposed that this is caused by the stress concentrations at the tips of asperities generating a crack path within the adhesive that is farther from the average adhesive-adherend interface [12–14]. Furthermore, increasing roughness makes the abrupt transition in elastic modulus more gradual as the asperities transfer load to the adhesive, thereby decreasing the average stress concentration for a crack propagating in a path at the tips of the asperities [12]. Both of these effects would tend to increase G_{th} with increasing R_a, but they still do not lead to a maximum followed by a decrease in G_{th} with increasing R_a. The effect of the abrupt change in modulus across a smooth adherend-adhesive interface is illustrated in Fig. 7, which shows the reduction in von Mises stress at the crack tip singular node in an aluminum ADCB joint at increasing distances from the interface. The data were from a 2-D elasto-plastic finite element model (ANSYS® 12, Ansys Inc., Canonsburg, PA, USA) using plane182 elements and singular elements to model the crack tip. The adhesive was modeled with a

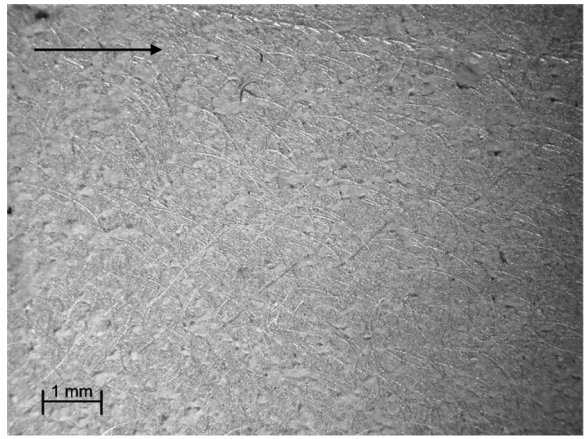

(a)

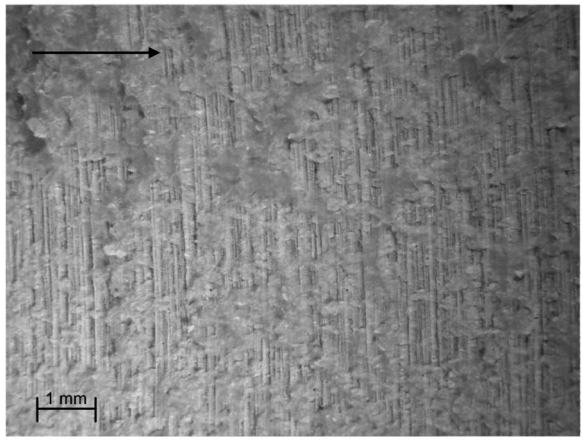

(b)

FIGURE 6 Fatigue failure surface of the thinner arm of an ADCB joint at (a) $R_a = 1.3\,\mu m$ and (b) $R_a = 3.9\,\mu m$. Crack propagation in the direction of the arrow.

multi-linear stress-strain curve derived from tensile tests [21]. The adherends were assumed to behave elastic-perfectly-plastic, with a tensile elastic modulus of $E = 68.9\,GPa$ and a tensile yield stress of $\sigma_y = 270\,MPa$. For the adhesive $E_a = 1.5\,MPa$ and $\sigma_y = 30\,MPa$.

Figure 7 shows that any mechanism that causes the crack to deviate from the interface can lower the stresses at the crack tip and improve the fatigue behavior.

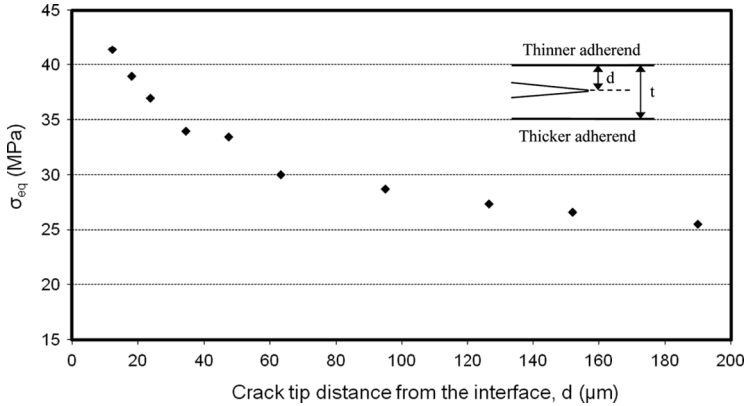

FIGURE 7 Von Mises stress at the crack tip as a function of the distance from the upper adherend smooth aluminum interface, d. Finite element predictions for an aluminum ADCB joint and at $G = 200\,\mathrm{J/m^2}$. The geometry of the ADCB joint was according to Fig. 1(b). t is the adhesive thickness equal to 380 μm.

Finally, crack growth is associated with the formation and development of a damage zone ahead of the crack [22]. The deviation of the crack path from the interface due to the increase in surface roughness may allow a larger volume of the adhesive to deform plastically and so increase the fracture energy.

In addition to the hypothesis that asperity tips can generate a crack path that is removed from the nominal interface, it has been proposed that at some value of roughness, the increased stress concentration at the tips of the asperities will reduce the fracture strength of adhesive joints [6]. Therefore, a combination of the mechanisms discussed in the section could possibly explain the observed maximum in G_{th} (Fig. 4).

3.1.3. Wettability and Void Formation

It has been shown that an increase in surface roughness can reduce the wettability of a substrate and, hence, the bond strength [23]. This effect would be accentuated if the adhesive is highly viscous, or if there was insufficient time for adhesive flow before curing, and it provides another mechanism by which a maximum G_{th}could arise (Fig. 4).

In present experiments, wetting was maximized by preheating both the adhesive and the aluminum to 55°C prior to adhesive application, and the bonded specimens were held at room temperature for at least 20 min before putting them in the oven for curing. These procedures were carried out to minimize the chance of the adhesive not wetting the substrate thoroughly.

To investigate whether the decrease in the G_{th} at $R_a = 9.0\,\mu m$ was due to an increase in void formation, a cross-section of the thinner arm of representative ADCB joints with $R_a = 1.9$, 6.4, and 9.0 μm were polished using a succession of abrasive papers (180-, 240-, 360-, 600-, 800-, and 1200-grit). The samples were then polished with 6-μm diamond paste followed by 1-μm colloidal silica and were carbon coated. Scanning electron microscopy failed to reveal any voids that might be associated with the valleys of the rougher specimens.

Increasing the surface roughness also raises the possibility of air entrapment when the adhesive is applied [12]. In addition, as the surface roughness increases, it becomes more likely that small pieces of aluminum may remain unattached or poorly attached to the substrate after cleaning. Indeed, the fatigue failure surfaces of specimens with $R_a \geq 6.4\,\mu m$ had some sites of interfacial failure (less than 5% of the fracture area) with embedded aluminum pieces in the adhesive fracture surface (Fig. 8). No interfacial failure was observed for $R_a < 6.4\,\mu m$. The number of interfacial fracture sites increased to 10–20% of the fracture area when the roughness increased to $R_a = 9.0\,\mu m$, suggesting that trapped air bubbles or weakly attached aluminum asperities may have caused some decrease in the fatigue performance of the specimens at $R_a = 9.0\,\mu m$.

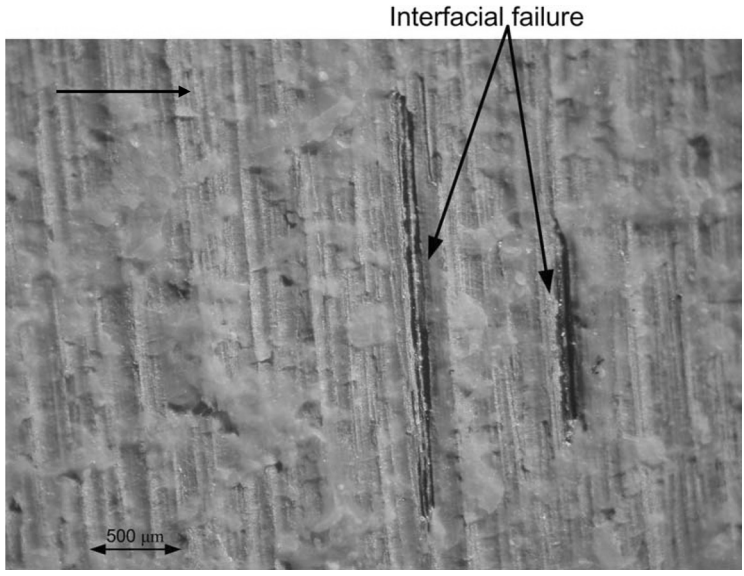

FIGURE 8 Some interfacial failures observed for a sample at $R_a = 6.4\,\mu m$. Crack propagation in the direction of the arrow.

It is concluded that the increase in G_{th} with surface roughness can come from several sources: an increase in the available bonding area, increased mechanical interlocking and crack growth retardation due to the substrate topography, and the deviation of crack path from the interface. However, at some roughness value, the crack path is far enough from the interface and, thus, no further increase in roughness affects the G_{th}. For very rough surfaces, the G_{th} drops again, which could be due to the possibility of local interfacial failures coming from void formation.

The crack growth rate graphs (da/dN *vs.* G) of aluminum ADCBs at $R_a = 1.3$, 3.9, and 9.0 μm are compared in Fig. 9. For clarity, only one representative test is shown at each roughness. It is seen that at relatively high crack growth rates, compared with threshold, the graphs tend to be indistinguishable. This is consistent with our earlier observation that the crack path moves farther from the interface as the crack speed increases [11,15], thereby becoming less sensitive to the surface roughness. This suggests that the effect of surface roughness should increase as the phase angle increases, and also as the crack speed slows near the threshold region. This hypothesis is examined in the next section using fatigue experiments on DCB joints under Mode I loading where the crack propagated near the mid-plane of the bondline.

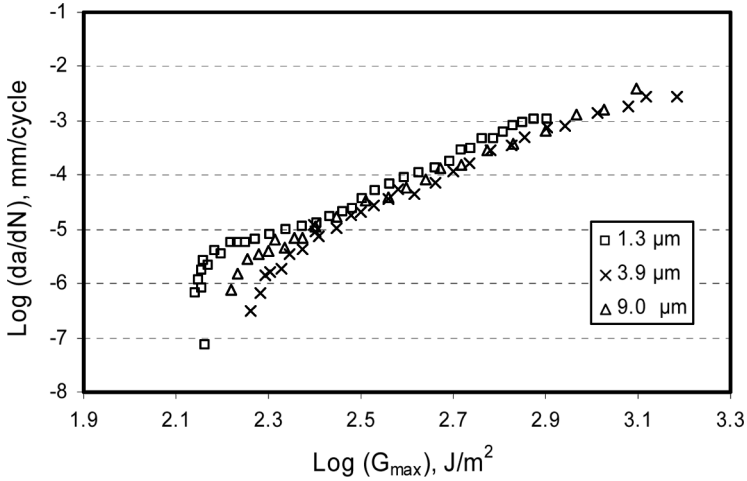

FIGURE 9 Fatigue crack growth rate of aluminum ADCB at $R_a = 1.3$, 3.9, and 9.0 μm.

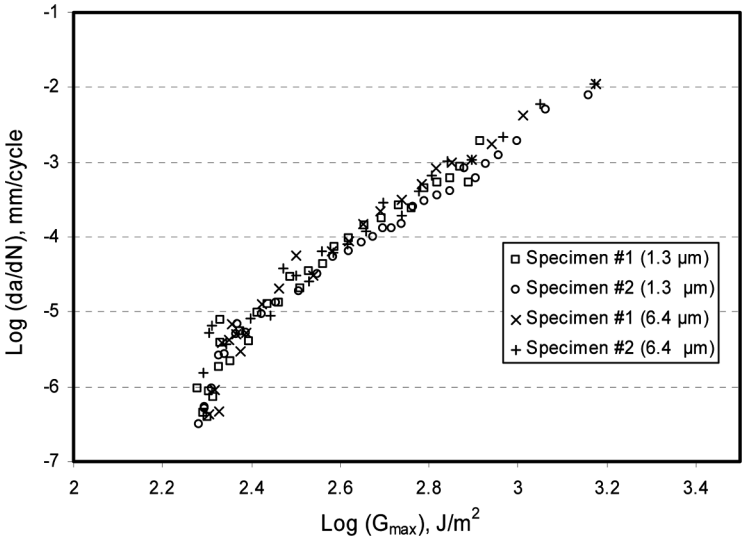

FIGURE 10 Effect of surface roughness on Mode I fatigue crack growth rates of aluminum DCB. Two representative experiments are shown for each roughness.

3.2. Mode-I DCB Specimens

Two roughness values were chosen for Mode I loading, $R_a = 1.3$, and 6.4 μm, corresponding to the two extreme values of the fatigue threshold under mixed-mode loading ($G_{th} = 121 \pm 12$ and $178 \pm 19\,\mathrm{J/m^2}$, respectively). Three experiments were conducted in each case, showing no statistically significant difference between the G_{th} values at the two roughnesses ($G_{th} = 195 \pm 3$ and $191 \pm 7\,\mathrm{J/m^2}$ at $R_a = 1.3$ and 6.4 μm, respectively). The crack growth rate graphs of two representative specimens for each roughness are compared in Fig. 10, showing no effect of roughness on the fatigue crack growth rates under Mode I loading. Therefore, consistent with the ADCB fatigue results at high crack speed, and as expected for cases where the crack path is far from the interface, no effect of surface roughness on the Mode I fatigue results was observed.

4. EFFECT OF SURFACE ROUGHNESS ON FRACTURE BEHAVIOR OF ADCB SPECIMENS

Compared with cyclic loading, quasi-static loading introduces a relatively high strain energy release rate and crack speed. It was shown

previously that quasi-static fracture tests at the same loading phase angle produce a more cohesive failure compared with fatigue threshold testing [11]. To verify further that surface roughness affects the behavior of an adhesive joint only when the crack path is very close to the interface, quasi-static fracture tests were conducted on aluminum ADCB joints.

The principal objective was to measure the critical strain energy release rate for initiation, G_c^i, and the steady-state critical strain energy release rate, G_c^s, as a function of surface roughness. The G calculation was the same as that used in the fatigue tests [15].

Fracture tests using ADCB specimens produced a typical R-curve [24,25]. After crack initiation at G_c^i, the first several crack growth sequences occurred at an increasing critical energy release rate, G_c, as the damage zone at the crack tip developed to its steady-state form [21] (Fig. 11). The steady state critical strain energy release rate, G_c^s, was considered to be the average value over the "plateau" (steady-state) region. The failure was fully cohesive in the adhesive (Fig. 12). Figure 13 shows the average G_c^i and G_c^s for the three tested roughnesses of $R_a = 1.3$, 1.9, and 6.4 μm. The error bars represent ±standard deviation calculated using the three measurements conducted for G_c^i at each R_a, while the number of data points used to calculate G_c^s was 96, 29, and 34 at R_a of 1.3, 1.9, and 6.4 μm,

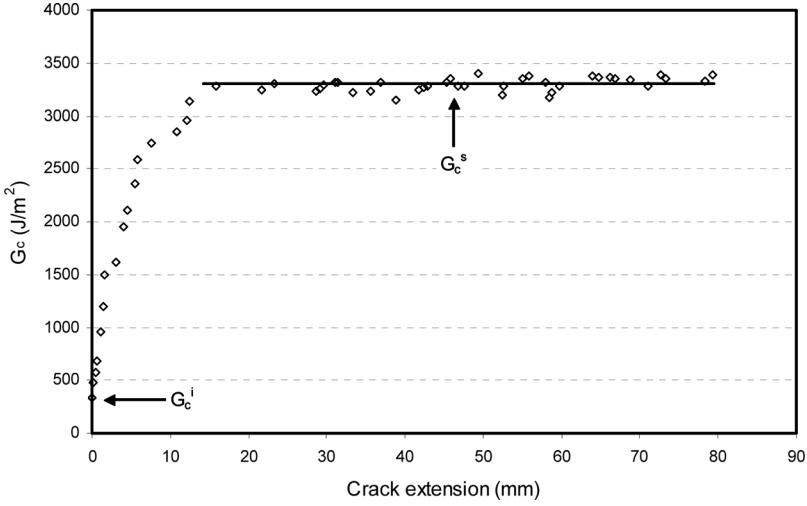

FIGURE 11 R-curve behavior of an ADCB joint at roughness of $R_a = 1.3$ μm.

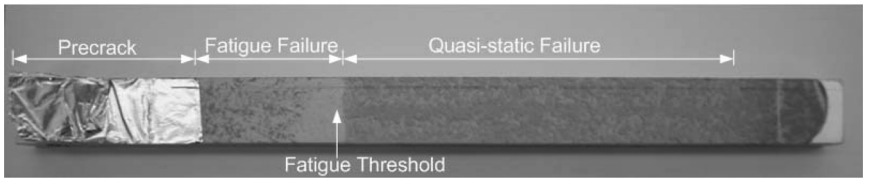

FIGURE 12 Fatigue and fracture failure surface of the thinner arm of an ADCB joint at $R_a = 1.3\,\mu m$.

respectively. It is clear that no effect of surface roughness was evident in G_c^i and G_c^s. Since the crack path in these fracture tests was relatively far from the interface (although still closer to the thinner adherend than the thicker one), this independency of fracture results on substrate roughness is consistent with the Mode I fatigue results and mixed-mode ADCB fatigue results at higher crack growth rates.

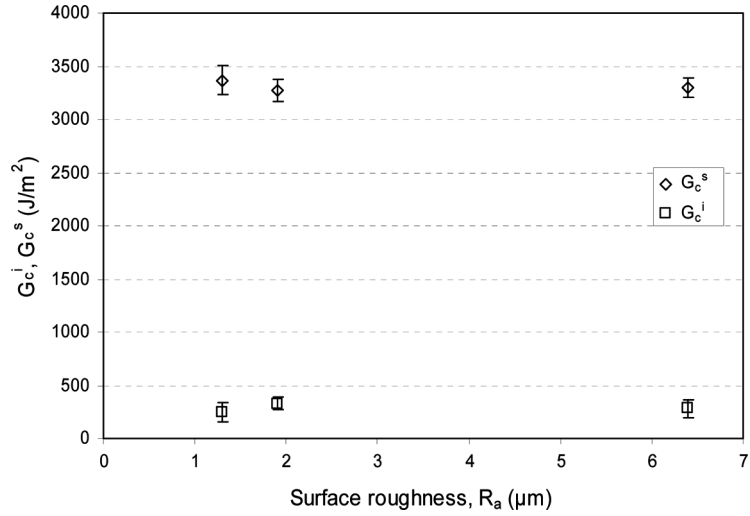

FIGURE 13 Effect of surface roughness, R_a, on the critical crack initiation strain energy release rate, G_c^i, and critical steady-state strain energy release rate, G_c^s, of ADCB joints. Given values are the average values (± 1 standard deviation). For G_c^i, three measurements were performed for each roughness. Number of data points on the plateau for G_c^s measurements at $R_a = 1.3$, 1.9, and 6.4 μm were 96, 29, and 34, respectively.

5. CONCLUSIONS

Surface roughness had a significant effect on G_{th} under a mixed-mode fatigue loading where the crack path was very close to the surface. The smallest G_{th} was measured for the lowest tested roughness, $R_a = 1.3\,\mu m$, and increased about 50% as the surface roughness was increased to $R_a = 3.9\,\mu m$. This maximum value was also measured at $R_a = 6.4\,\mu m$, but then decreased 20% for a very rough surface of $R_a = 9.0\,\mu m$.

The increase in G_{th} with surface roughness up to $R_a = 3.9\,\mu m$ could be attributed to several factors: increase in bonding and fracture surface area, crack growth retardation due to crack path deflection around asperities, and a shift in the failure locus away from the interface caused by stress concentrations at the tips of roughness asperities. This last effect is hypothesized to keep the crack tip away from regions of stress concentration closer to the aluminum-adhesive interface, where crack path propagation would otherwise occur more easily. The insensitivity of G_{th} to roughness for $3.9\,\mu m \leq R_a \leq 6.4\,\mu m$ could be due to the crack path being far enough from the interface to be insensitive to these effects of substrate roughness.

The decrease in G_{th} at $R_a = 9.0\,\mu m$ was attributed to the increase in stress concentration at the tip of the roughness asperities, and also to void formation resulting from entrapped air and possibly weakly attached asperities.

Under mixed-mode loading, the effect of surface roughness on the fatigue crack growth rate decreased as the crack growth rate increased. This was due to the crack path shifting farther from the interface as the strain energy release increased.

Experimental results for Mode I fatigue, both the fatigue threshold and the fatigue crack growth rates, and quasi-static fracture, both G_c^i and G_c^s, showed no dependency on the surface roughness. This was due to the crack path being relatively far from the interface and well within the adhesive.

The use of a different substrate material and roughening procedure might affect the microtopography and wettability of the bonding surface and, hence, produce different results. However, an indication of the generality of the present observations is provided by the fact that similar trends have been reported in the literature with steel joints and other adhesives. For example, as mentioned previously, References [7] and [8] found optimum R_a values in cases where failure after quasi-static loading was close to the interface and was, thus, affected by the roughness. The torsional fatigue life of steel joints was also found to exhibit a maximum at a particular R_a [9].

It is concluded that surface roughness has an appreciable effect only when the crack growth rate is low under mixed-mode loading *i.e.*, near the fatigue threshold. Under these conditions, the optimum roughness increased G_{th} by up to 50%. At relatively high phase angles, the effect of roughness may become pronounced at crack growth rates larger than the fatigue threshold.

ACKNOWLEDGMENTS

The authors acknowledge the Natural Sciences and Engineering Research Council of Canada, the Ontario Centres of Excellence, and General Motors of Canada for their financial support.

REFERENCES

[1] Critchlow, G. W. and Brewis, D. M., *Int. J. Adhes. Adhes.* **15**, 173–176 (1995).
[2] Harris, A. F. and Beevers, A., *Int. J. Adhes. Adhes.* **19**, 445–452 (1999).
[3] Shahid, M. and Hashim, S. A., *Int. J. Adhes. Adhes.* **22**, 235–244 (2002).
[4] Zhang, S. Panat, R. and Hsia, K. J., *J. Adhes. Sci. Technol.* **17**, 1685–1711 (2003).
[5] Tzetzis, D., *J. Mater. Sci.* **43**, 4271–4281 (2008).
[6] Prolongo, S. G., Rosario, G., and Urena, A., *J. Adhesion Sci. Technol.* **20**, 457–470 (2006).
[7] Sekercioglu, T., Rende, H., Gulsoz, A., and Meran, C., *J. Mater. Process. Technol.* **142**, 82–86 (2003).
[8] Uehara, K. and Sakurai, M., *J. Mater. Process. Technol.* **127**, 178–181 (2002).
[9] Lee, D. G. Kim, K. S. and Im, Y.-T., *J. Adhes.* **35**, 39–53 (1991).
[10] Kwon, J. W. and Lee, D. G., *J. Adhes. Sci. Technol.* **14**, 1085–1102 (2000).
[11] Azari, S., Papini, M., Schroeder, J. A., and Spelt, J. K., Fatigue threshold behavior of adhesive joints. *Int. J. Adhes. Adhes.* **30**, 145–159 (2010).
[12] Packham, D.E., The mechanical theory of adhesion – A seventy year perspective and its current status, in *1st International Congress on Adhesion Science and Technology: Invited Papers*, W. J. Van Ooij and H. R. Anderson (Eds.) (VSP Publishers, Utrecht, 1998), pp. 81–108.
[13] Evans, J. R. G. and Packham, D. E., *J. Adhes.* **10**, 177–191 (1979).
[14] Hine, P. J., El Muddarris, S., and Packham, D. E., *J. Adhes.* **17**, 207–229 (1984).
[15] Azari, S., Papini, M., Schroeder, J. A., and Spelt, J. K., *Eng. Fract. Mech.* **77**, 395–414. (2010).
[16] Wegman, R. F., *Surface Preparation Techniques for Adhesive Bonding*, (Noyes Publications, New Jersey, 1989), Ch. 2, pp. 27–30.
[17] Davies, P., *Protocols for Interlaminar Fracture Testing of Composites*, (European Structural Integrity Society: Polymer and Composites Task Group, Plouzane, France 1992).
[18] ASTM E647, Standard test method for measurement of fatigue crack growth rates, (American Society for Testing and Materials, West Conshohocken, PA 2000).
[19] Fernlund, G. and Spelt, J. K., *Comp. Sci. Technol.* **50**, 441–449 (1994).
[20] ISO 4287, Surface roughness – Terminology – Part 1: Surface and its parameters, (International Organization for Standardization, Geneva, Switzerland 1984).

[21] Azari, S., Papini, M., and Spelt, J. K., Effect of adhesive thickness on fatigue and fracture of toughened epoxy adhesive joints – Part II. Analysis and finite element modeling, *Eng. Fract. Mech.* submitted.
[22] Hunston, D. L., Kinloch, A. J., and Wang, S. S., *J. Adhes.* **28**, 103–114 (1989).
[23] Hitchcock, S. J., Carroll, N. T., and Nicholas, M. G., *J. Mater. Sci.* **16**, 714–732 (1981).
[24] Hutchinson, J. W. and Suo, Z., Mixed mode cracking in layered materials, in J. W. Hutchison and T. Y. Wu (Eds.) (Academic Press Inc., New york, 1992), Vol. 29, pp. 63–191.
[25] Azari, S., Eskandarian, M., Papini, M., Schroeder, J. A., and Spelt, J. K., *Eng. Fract. Mech.* **76**, 2039–2055 (2009).